AUT Journal of Electrical Engineering

AUT J. Elec. Eng., 55(3) (Special Issue) (2023) 333-350
DOI: 10.22060/eej.2023.22068.5510

Experimental Validation of Adaptive Sliding Mode Fuzzy Controller for an Inertially Stabilized Platform

M. Nikkhoo*[1], H. Sayyaadi[2], M. S. Seif[2]

[1] Kish International Campus of Sharif University of Technology, Kish, Iran.

[2] School of Mechanical Engineering, Centre of Excellence in Hydrodynamics and Dynamics of Marine Vehicles, Sharif University of Technology, Tehran, Iran.

ABSTRACT: The adaptive fuzzy control algorithm using the novel membership function was designed to suppress chattering phenomena in the performance of the three-axis Inertially Stabilized Platform (ISP) applied to the stabilization and tracking of the line of sight in optical cameras mounted on a moving boat. The stability of the nonlinear controller was proven through the Lyapunov method. For the theoretical evaluation of the controller performance, a series of numerical simulations were performed. The nonlinear kinematic and dynamic equations of the ISP were derived for this purpose. Due to the coupling between ISP frames, direct implementation of the suggested controller was not feasible. To this end, four simplified assumptions were applied to the ISP design. To evaluate the performance of the proposed control algorithm, both numerical simulation and experimental methods were used on the three-axis ISP, and the results of both methods were compared and validated. Further, the results of the proposed nonlinear control algorithm were compared with the optimal PID linear algorithm. Besides, experimentally obtained angular velocities of a boat were used for the base motion of the ISP in the numerical simulations. Despite the existence of uncertainties in dynamic system modeling, the outcomes of the implementation of the control algorithm and experimental tests indicated that the adaptive fuzzy sliding mode algorithm stabilized the line of sight with acceptable accuracy and improved its performance in suppressing chattering phenomena.

Review History:

Received: Dec. 28, 2022
Revised: Mar. 06. 2023
Accepted: May, 02, 2023
Available Online: Dec. 01, 2023

Keywords:

Inertial navigation
Target tracking
Cameras
Fuzzy logic
Adaptive control
Stabilization

1- Introduction

Vibrations of the base of the devices that carry optical, telecommunication, measurement, and weapon systems reduce efficiency, measurement accuracy, and subsequently errors in the measurement results of these systems. One way to avoid such errors is to actively isolate devices from the vibrations of the base by stabilizing platforms. Based on the degrees of freedom in the angular movement of ISP platforms, stabilization devices are divided into one, two [1], and three-axis [2] types. ISP platforms are used to stabilize images taken by the camera mounted on the power transmission inspector bird [3, 4]. In addition, visual-based controllers have been addressed in some previous research [5].

So far, many studies in this field have designed control algorithms for ISP stabilization and tracking. Conventional linear controllers such as PID, Lead-Lag, and least mean square-based active disturbance rejection control [6] have been used in most engineering applications. The main advantage of these kinds of controllers is that they are easy to implement and have simple processors. However, due to their limited performance, their applicability is somewhat limited. External disturbances such as friction and mass imbalance, as well as dynamic coupling between axes, undermine the performance of control algorithms.

Dynamic coupling between axes is another major challenge in designing a controller for the ISP. The previous study [4] used the Internal Model Control (IMC) algorithm and system linearization to simplify the dynamic system and two-axis dynamic coupling, as well as the reverse dynamic system in designing the controller. Thus, the dynamic two-input, two-output system with two-axis coupling (MIMO controller) was transformed into two single-input, single-output (SISO) systems. The authors in [7] applied a dual-rate-loop control algorithm based on a disturbance observer of angular acceleration to eliminate disturbances in the stabilization loop. There is a critical need to use other control algorithms with variable structures over time. This is because uncertainty in dynamic system modeling results in different optimal parameters for different dynamic systems.

Besides the advantages of the robust controller, this controller has two main limitations: 1) The implementation of the H∞ controller is quite intricate and requires advanced processors, and 2) Since their design is conservative due to disturbances, the system's performance has various

*Corresponding author's email: mohammadnickhoo@gmail.com

limitations. The authors in [8] investigated the possibility of designing an optimal robust controller using the H∞ method on the dynamic model of the platform, but they did not report the improvement of the system response. To address this challenge, a higher-order sliding mode observer (HOSMO) was developed [9] to estimate the uncertainties and states of the system and design the terminal sliding mode control rule. One of the challenges in designing the active disturbance rejection controller (ADRC) was the presence of sensor noise, which reduced the controller's robustness to uncertainties. A study [10] has proposed the use of a combination of the ADRC and Noise Reduction Disturbance Observer (NRDO) to eliminate disturbances and noises associated with encoders and uncertainties associated with parameter measurements. Unfortunately, these works used a linear dynamic model in their controller design process. To design the controller for nonlinear systems and to be able to generalize the system parameters, the Sliding mode and Backstepping design methods have been used.

The sliding mode controller is a variable structure control method. However, the responses of the control system do not change due to disturbances and changes in dynamic system parameters. Thus, its advantage is its non-sensitivity to disturbances and noise and its disadvantage is its performance in actual conditions. Some studies used the sliding mode control algorithm to stabilize the platform [11, 12]. Due to the robustness of the sliding mode controller, it has been discussed in the literature [13]. Furthermore, using the continuous finite-time sliding mode control method, a control algorithm was designed to eliminate the chattering phenomenon which is the main limitation of the Sliding mode method in the stabilization of the dynamic system [12]. The conventional backstepping nonlinear control algorithm has been discussed in some ISP literature [11, 14, 15] to stabilize the platform. Its advantage over the sliding mode method is the reduction of the chattering phenomenon in the controller design. Despite the effectiveness of the Backstepping algorithm, adaptive sliding mode algorithms have been shown to exhibit a more appropriate response. As a result, the controller proposed in this study has also been designed based on adaptive sliding mode algorithms.

A well-known feature of fuzzy control is its simplicity of design and ability to overcome uncertainties. Because fuzzy rules express the knowledge and experience of experts linguistically, they are preferred over classical control methods [16]. An important feature of fuzzy systems is their ability to approximate any nonlinear, indefinite, and uncertain function [17]. The different fuzzy control techniques (fuzzy type-1 and type-2) and their hybrid forms (adaptive hybrid fuzzy controller and PID fuzzy controller) in ISPs were also discussed [18]. In [19], MIMO multi-input fuzzy control algorithms have also been used to stabilize ISPs.

Another method of solving the challenges of uncertainty of system parameters, mentioned in the literature, is to implement adaptive algorithms. The Radial basis function neural network (RBFNN) adaptive neural network algorithm has been used in [1, 14, 20]. The adaptive control algorithm of the neural network has been used as well as the extended state observer [1] to design a control system to improve the stabilization accuracy and speed of the platform dynamic response due to the nonlinear dynamics of the platform and changes in the structure of the platform over time. Adaptive controls based on RBFNN are presented in [20] for improving the precision of attitude stabilization. Its method was based on estimating disturbance torques. Adaptive control based on RBFNN is shown to have a more fluent control voltage than state feedback control according to the results of the proposed controller [20]. Research has also addressed the stabilization of the platform using a combined PID model and Model Reference Adaptive Control (MRAC) [21] to design a controller to eliminate mass imbalance disturbances loaded onto the ISP in a time-varying and non-linear manner.

This study implements a combination of fuzzy-adaptive and sliding mode controllers, which was first introduced in [19] for a complex ISP considering all coupling terms of three-axis dynamics. The main objective of the controller design was to compensate for the effect of base motion on the ISP's performance, which was not addressed in the previous study [19]. In addition to the fact that the controller in this study is the same as that in [19], the stability of the algorithm has been verified by applying the Lyapunov theorem due to the following two factors: (1) our dynamic equations differ from those in [19], and (2) we designed the controller for three axes separately (roll, pitch, and yaw), while the controller in [19] was designed for the roll axis in three perpendicular directions. Four assumptions were imposed on the design of ISP to simplify the dynamic equations. These assumptions are characterized by the fact that they are very close to reality and simplify the dynamic equations of ISP. In addition, due to technological limitations (electrical motors), we chose the controller's parameters such that the driving torque remained within a reasonable range. In this paper, there are two terms of the control algorithm: fuzzy and adaptive sliding mode controllers. The fuzzy controller is designed to generate torque corresponding to errors in the positions and velocities of ISP gimbals to solve the chattering challenge. In addition, dynamic coupling between the axes is considered in the design of the fuzzy controller. The sliding mode controller was designed based on the "s" parameter, which is defined as a representative of these errors, and it is defined in equation (21). Moreover, the parameter "s" is used as an input for the fuzzy controller. Low "s" values cause the fuzzy controller to generate proportional torque that does not lead to the chattering phenomenon. In both fuzzy and sliding mode controllers, adaptive structures are used to address the uncertainties of parameters and their change over time. The derivatives of fuzzy control parameters are proportional to the "s" parameters. The outline of the paper is organized as follows: Section 2 explains the nonlinear dynamic equations of the 3-axis ISP and their simplified assumptions. Section 3 describes an adaptive fuzzy sliding mode controller and its stability is proved by the Lyapunov theorem. In Section 4, the results of numerical simulation are presented and compared with the experimental tests. Finally, conclusions are presented

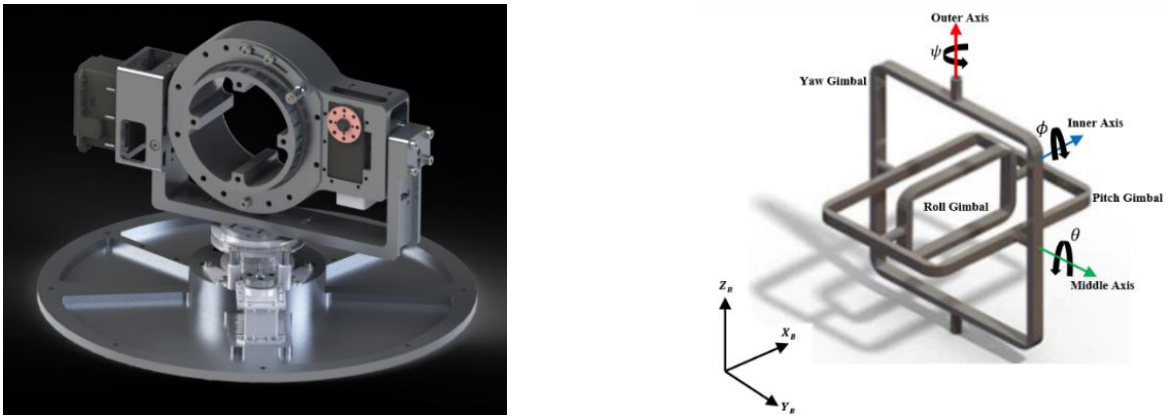

(a) (b)

Fig. 1. (a) Schematic of three-axis gimbal platform, (b) Kinematics of 3-axis gimbal platform. Definition of Roll, Pitch, and Yaw axis.

in the last section.

2- Dynamic Modeling of Three-Axis Stabilized Platform

The kinematic model of the system includes four members in three-axis stabilized platform modeling (Figure 1): Gimbal platform, Yaw gimbal, Pitch gimbal, and Roll gimbal. All members are assumed to be rigid and each has a separate coordinate system. A torque motor and an angle sensor are connected to each gimbal on its axes. An Attitude and Heading Reference System (AHRS) sensor is used to measure the absolute angular movements of the stable platform.

2- 1- Kinematic Relations

The structure of the three-axis gimbal platform is presented in Fig. 1 As shown, four reference coordinate systems including the gimbal attached to body B, and three gimbals of Y, P, and R, which are fixed to the yaw, pitch, and roll axes, have been used to describe the stabilizing performance. These rotation angles are defined as vectors $[\phi\ \theta\ \psi]^T$ for the roll, pitch, or yaw axis, respectively. For coordinates of each axis, subscripts of "R", "P", "Y", and "B" were used for roll, pitch, yaw, and body axis, respectively. Given that there are measurement sensors on the carrier, therefore it is defined as:

$$\omega = [p \quad q \quad r]^T \tag{1}$$

The angular velocity of all axes in the inertial monitoring device is calculated according to the parameters in Eq. (3) and the angles $[\phi\ \theta\ \psi]^T$. The angular accelerations of each gimbal can be calculated through derivation of the angular velocity relations associated with that gimbal as follows:

$$\dot{\omega}_{IB}^{B} = [\dot{p} \quad \dot{q} \quad \dot{r}]^T \tag{2}$$

$$\dot{\omega}_{IY}^{Y} = [c_\psi(\dot{p} + q\dot{\psi}) + s_\psi(\dot{q} - p\dot{\psi}) \quad c_\psi(\dot{q} - p\dot{\psi}) - s_\psi(\dot{p} + q\dot{\psi}) \quad \dot{r} + \ddot{\psi}]^T \tag{3}$$

$$\dot{\omega}_{IP}^{P} = \frac{d}{dt}(\omega_{IY}^{P} + \begin{bmatrix}0\\ \dot{\theta}\\ 0\end{bmatrix}) \tag{4}$$

$$\dot{\omega}_{IR}^{R} = \frac{d}{dt}(\omega_{IP}^{R} + \begin{bmatrix}\dot{\phi}\\ 0\\ 0\end{bmatrix}) \tag{5}$$

2- 2- Friction Modeling

The friction of the roll, pitch, and yaw axes are modeled using Eq. (6) as follows:

$$Friction = D \times \dot{\theta}_i + F \times (sgn\ \dot{\theta}_i) \tag{6}$$

Where D: Viscous friction between axial components (roll, pitch, and yaw), $F \times (sgn\ \dot{\theta}_i)$: Coulomb friction and static friction representative function (related to wire tension), $\dot{\theta}_i$: Relative angular velocity of the (roll, pitch, and yaw) axes.

2- 3- Dynamic Equations of the Gimbals

The dynamic equations of the stabilized platform are extracted from ref [19], through the Newton–Euler method. According to the extracted dynamic equations in Appendix A1 and the equation related to the mentioned system, the relations between the relative angular acceleration of the axes and the torques of the motors are represented in Equations (7). The parameters used in Equations (7) are defined in Appendix A1:

$$\ddot{\psi} = \frac{A_{P\theta}A_{Y\phi}MXR + A_{R\phi}A_{Y\theta}MYP - A_{P\theta}A_{R\phi}MZY}{A_{p\psi}A_{R\phi}A_{Y\theta} - A_{P\theta}A_{R\phi}A_{Y\psi} + A_{P\theta}A_{R\psi}A_{Y\phi}} \quad \text{(a)}$$

$$\ddot{\theta} = \frac{-A_{p\psi}A_{Y\phi}MXR + \left(A_{R\psi}A_{Y\phi} - A_{R\phi}A_{Y\psi}\right)MYP + A_{p\psi}A_{R\phi}MZY}{A_{p\psi}A_{R\phi}A_{Y\theta} - A_{P\theta}A_{R\phi}A_{Y\psi} + A_{P\theta}A_{R\psi}A_{Y\phi}} \quad \text{(b)} \qquad (7)$$

$$\ddot{\phi} = \frac{A_{p\psi}A_{Y\theta}MXR - A_{P\theta}A_{Y\psi}MXR - A_{R\psi}A_{Y\theta}MYP + A_{P\theta}A_{R\psi}MZY}{A_{p\psi}A_{R\phi}A_{Y\theta} - A_{P\theta}A_{R\phi}A_{Y\psi} + A_{P\theta}A_{R\psi}A_{Y\phi}} \quad \text{(c)}$$

2- 4- Simplifying Dynamic equations

To design a control system and prove its stability, the dynamic equations of nonlinear and coupled motion should be somewhat simplified. This section represents simplified dynamic motion calculations.

Assumption 1: Following Eq. (8), assume the roll axis is designed such that the moments of inertia of two axes perpendicular to their motions are equal:

$$I_{R_y} = I_{R_z} \qquad (8)$$

Assumption 2: The 3D design of the three-axis ISP is developed in such a way that Eq. (9) is established.

$$I_{Y_z} > I_{P_x} \qquad (9)$$

Assumption 3: In the 3D design of the three-axis ISP, the order of the magnitude of the value of A_{Y_ψ} is 10^{-3} and the value of the parameter $I_{R_x}.\sin^2\theta$ is of the order of 10^{-3} or less. Therefore, in calculations and to prove stability, the following approximation should be used:

$$A_{Y_\psi} - I_{R_x}.\sin^2\theta \simeq A_{Y_\psi} \qquad (10)$$

Assumption 4: Since the ISP is mounted on a boat on the sea, the motion of the base of the three-axis ISP in the various tests is such that the angle of the pitch axis with respect to the horizontal line (perpendicular to the direction of gravity) is in the relational range (11). To stabilize and track the target in the horizontal line, it is necessary to stabilize the pitch angle around the value of $-\theta_{pitch}$:

$$0 < \theta_{pitch} < 10° = 0.1745 \text{ (rad)} \qquad (11)$$

By applying the above assumptions and using equations (7), the simplified equations are stated as follows:

$$\ddot{\theta} = \frac{MYP}{I_{P_y} + I_{R_y}} \quad \text{(a)}$$

$$\ddot{\phi} = \frac{A_{Y_\psi}}{I_{R_x}\left(A_{Y_\psi} - I_{R_x}.\sin^2\theta\right)}.MXR + \frac{\sin\theta}{A_{Y_\psi} - I_{R_x}.\sin^2\theta}.MZY \quad \text{(b)} \qquad (12)$$

$$\ddot{\psi} = \frac{1}{A_{Y_\psi} - I_{R_x}.\sin^2\theta}.MZY + \frac{\sin\theta}{A_{Y_\psi} - I_{R_x}.\sin^2\theta}.MXR \quad \text{(c)}$$

Where all parameters used in the above equations including MXR, MYP, and MZY are defined in Appendix A1.

2- 5- Checking the Action Control Coefficient Sign

System controllability requires a non-zero (or single signal) action control coefficient. Accordingly, to determine the sign of the MXR, MYP, and MZY coefficients (or $\tau_Y.\tau_P.\tau_R$ torque coefficients in equations (12)), we will have:

$$A_{Y_\psi} - I_{R_x}.sin^2\theta = \underbrace{I_{Y_z} - sin^2\theta\,.I_{P_x}}_{>0\ \ Assumption\ 2} + \underbrace{cos^2\theta\left(I_{P_z} + I_{R_y}\right)}_{>0} \qquad (13)$$

$$A_{Y_\psi} - I_{R_x}.\sin^2\theta \simeq I_{Y_z} + I_{P_z} + I_{R_z\,\text{يا}\,R_y} > 0$$
$$A_{Y_\psi} - I_{R_x}.\sin^2\theta \simeq A_{Y_\psi} > 0 \qquad (14)$$

$$0 < \theta_{pitch} < 10° \implies -10 < \theta < 0 \implies \sin\theta < 0 \qquad (15)$$

3- Designing an Adaptive Fuzzy Sliding Mode Controller and Proving the Stability

3- 1- Designing Controller

Following the definition for each of the variables ϕ,θ,ψ , we will have:

$$e = \begin{bmatrix} \phi - \phi_d \\ \theta - \theta_d \\ \psi - \psi_d \end{bmatrix} \tag{16}$$

$$s = \dot{e} + [c]e \tag{17}$$

Where ϕ_d ,θ_d ,ψ_d are the desired values of angles. Hence, through calculating the derivative of the Eq. (17) we will have:

$$\begin{bmatrix} \ddot{\phi} \\ \ddot{\theta} \\ \ddot{\psi} \end{bmatrix} = \begin{bmatrix} \ddot{\phi}_d \\ \ddot{\theta}_d \\ \ddot{\psi}_d \end{bmatrix} + \dot{s} - \begin{bmatrix} c_1 & 0 & 0 \\ 0 & c_2 & 0 \\ 0 & 0 & c_3 \end{bmatrix} \dot{e} \tag{18}$$

By replacing Eq. (12) into matrix form, we will have:

$$\begin{bmatrix} \ddot{\phi} \\ \ddot{\theta} \\ \ddot{\psi} \end{bmatrix} = [F]. \begin{Bmatrix} MXR \\ MYP \\ MZY \end{Bmatrix} \tag{19}$$

By combining equations (18) and (19) we will have:

$$[F] \begin{Bmatrix} \tau_R \\ \tau_P \\ \tau_Y \end{Bmatrix} = -[F].\{V\} + \begin{Bmatrix} \ddot{\phi}_d \\ \ddot{\theta}_d \\ \ddot{\psi}_d \end{Bmatrix} + \dot{s} - [c]\dot{e} \tag{20}$$

Where $\{V\}$ is defined as follows:

$$\{V\} = \begin{Bmatrix} MXR \\ MYP \\ MZY \end{Bmatrix} - \begin{Bmatrix} \tau_R \\ \tau_P \\ \tau_Y \end{Bmatrix} \tag{21}$$

According to the Equations (12-a) to (12-c) and the definition of the matrix F in Equation (19), we have:

$$[F] = \begin{bmatrix} \frac{1}{I_{R_x}} & 0 & \frac{\sin\theta}{I_{Y_z} + I_{P_z} + I_{R_z}} \\ 0 & \frac{1}{I_{P_y} + I_{R_y}} & 0 \\ \frac{\sin\theta}{I_{Y_z} + I_{P_z} + I_{R_z}} & 0 & \frac{1}{I_{Y_z} + I_{P_z} + I_{R_z}} \end{bmatrix} \tag{22}$$

Following Eq. (22), the determinant of the matrix F is positive, so this matrix is invertible.

$$\begin{aligned} \det(F) &= \frac{1}{I_{R_x}.\left(I_{P_y} + I_{R_y}\right).\left(I_{Y_z} + I_{P_z} + I_{R_z}\right)} \\ &- \frac{\sin^2(\theta)}{\left(I_{P_y} + I_{R_y}\right)\left(I_{Y_z} + I_{P_z} + I_{R_z}\right)^2} \\ &= \underbrace{\frac{1}{\left(I_{P_y} + I_{R_y}\right).\left(I_{Y_z} + I_{P_z} + I_{R_z}\right)}}_{>0} \times \\ &\underbrace{\left(\frac{1}{I_{R_x}} - \frac{\sin^2(\theta)}{I_{Y_z} + I_{P_z} + I_{R_z}}\right)}_{>0} \end{aligned} \tag{23}$$

By defining $G = [F]^{-1}$ and using Eq. (20), we will have:

$$G\dot{s} = \begin{Bmatrix} \tau_R \\ \tau_P \\ \tau_Y \end{Bmatrix} + \{V\} + \mathrm{G}\left([c]\dot{e} - \begin{Bmatrix} \ddot{\phi}_d \\ \ddot{\theta}_d \\ \ddot{\psi}_d \end{Bmatrix} \right) \tag{24}$$

On the other hand, we define the control rule as Eq. (25) as pointed out in the literature [15, 19]. The u_o part is the output of the compensating controller and the u_c part is the output of fuzzy controller.

$$\begin{aligned} &\begin{Bmatrix} \tau_R \\ \tau_P \\ \tau_Y \end{Bmatrix} = -(\{u_o\} + \{u_c\}) = \\ &-\left[\begin{Bmatrix} u_{o_R} \\ u_{o_P} \\ u_{o_Y} \end{Bmatrix} + \begin{Bmatrix} u_{c_R} \\ u_{c_P} \\ u_{c_Y} \end{Bmatrix} \right] \end{aligned} \tag{25}$$

$$u_o = ([a] + [\sigma]_s)s \tag{26}$$

$$u_c = \begin{bmatrix} u_{c_1} \\ u_{c_2} \\ u_{c_3} \end{bmatrix} = [f]_{adap}\{u_f\} \tag{27}$$

In equations (26, 27), the parameter $[a]$ is constant, and the parameters $[\sigma]_s$ and $[f]_{adap}$ are calculated through the matching rules presented in Equations (28, 29). Block diagram of the designed controller is illustrated in Fig. 2.

$$\dot{f}_{ij} = \gamma_{ij} s_i u_{fi} \tag{28}$$

$$\dot{\sigma}_i = \eta_i s_i^2 \tag{29}$$

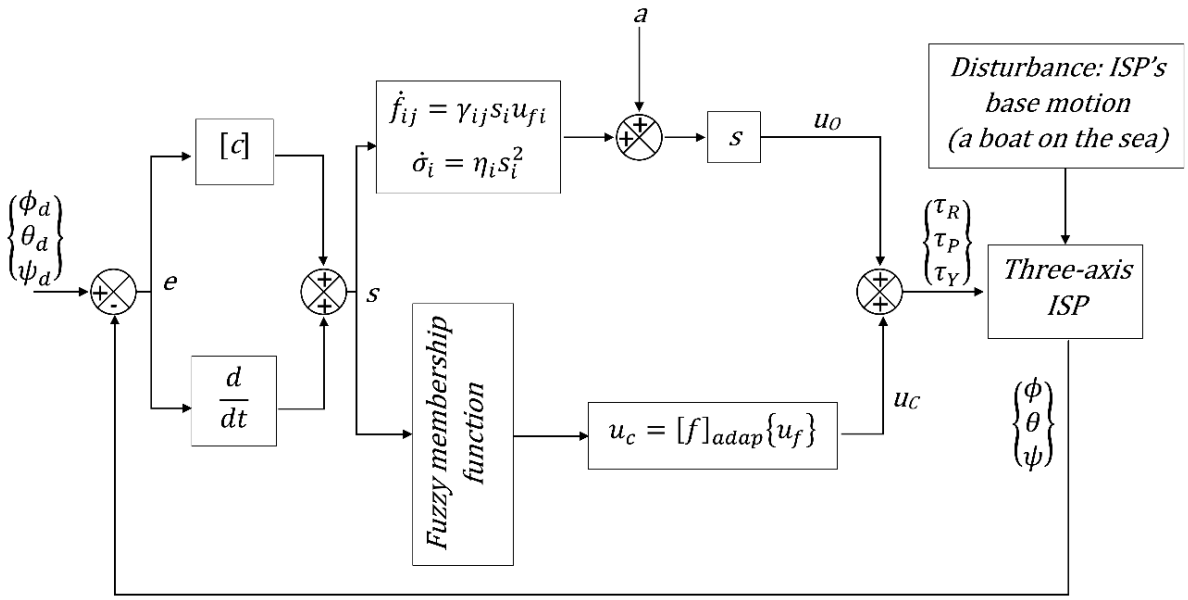

Fig. 2. Block diagram of the proposed combination of adaptive fuzzy controller and sliding mode algorithm.

3- 2- Proving the Stability

In this article, we provide evidence for the stability of the ISP based on the reference [22]. Our approach to proving controller stability differs from that of [22] in that the proposed controller is designed for three axes (roll, pitch, yaw) separately, while [22] designed the controller for three perpendicular directions of the roll frame axis. The control system in the mentioned study is represented for adjusting the angle of the roll axis in three directions. This study, however, uses it to control the roll, pitch, and yaw axes separately. Thus, it is necessary to re-examine the proof of stability. To prove the stability of the control rule, the Lyapunov function is defined as follows:

$$V = \underbrace{s^T G s}_{V_1} + \frac{1}{2}\sum\sum\frac{1}{\gamma_{ij}}\tilde{f}_{ij}^2 + \frac{1}{2}\sum_{i=1}^{n}\frac{1}{\eta_i}\tilde{\sigma}_i^2 \qquad (30)$$

The derivative of section V_1 is divided as follows:

$$\dot{V}_1 = \dot{s}^T G s + s^T \dot{G} s + s^T G \dot{s} \qquad (31)$$

By defining "w" and "B" according to equations (33, 34), we will have:

$$\dot{V}_1 = s^T\left(w\dot{s}^T G s + \dot{G} s + G\dot{s}\right) = s^T\left(B + \begin{Bmatrix}\tau_R\\ \tau_P\\ \tau_Y\end{Bmatrix}\right) = s^T(B - u_o - u_c) = s^T[B - (a+\sigma)s - u_c] \qquad (32)$$

The parameters used in Eq. (31) are the same as the parameters in Equations (32) and (33):

$$w = [\,1/3s_1 \;\; 1/3s_2 \;\; 1/3s_3\,]^T \qquad (33)$$

$$B = w\dot{s}^T G s + \dot{G} s + G\dot{s} - \begin{Bmatrix}\tau_R\\ \tau_P\\ \tau_Y\end{Bmatrix} = w\dot{s}^T G s + \dot{G} s + G\left([c]\dot{e} - \begin{Bmatrix}\ddot{\phi}_d\\ \ddot{\theta}_d\\ \ddot{\psi}_d\end{Bmatrix}\right) + \{V\} \qquad (34)$$

Thus, the derivative of Lyapunov function will be expressed via Eq. (35):

$$\dot{V} = \dot{V}_1 + \sum_{i=1}^{3}\sum_{j=1}^{3}\frac{1}{\gamma_{ij}}\tilde{f}_{ij}\dot{\tilde{f}}_{ij} + \sum_{i=1}^{3}\frac{1}{\eta_i}\tilde{\sigma}_i\dot{\tilde{\sigma}}_i$$
$$= \sum_{i=1}^{3} s_i(B_i - a_i s_i - \sigma_i s_i - u_{ci}) + \quad (35)$$
$$\sum_{i=1}^{3}\sum_{j=1}^{3}\frac{1}{\gamma_{ij}}\tilde{f}_{ij}\dot{\tilde{f}}_{ij} + \sum_{i=1}^{3}\frac{1}{\eta_i}\tilde{\sigma}_i\dot{\tilde{\sigma}}_i$$

In Eq. (35), parameter B_i represents the rows of vector B. According to [19], due to the definition of u_o in equation (26), the tracking error of the system approaches zero asymptotically. As a result, all of the terms of relation (34) are bounded including s , $\dot{s}$, G , $\dot{G}$, and second derivatives of desired angles. Vector "V" in equation (34), as defined as equation (21) is a function of angles and their rates, therefore this term is also bounded, and thus all B_i are bounded. If f_{ij}^* is defined as the optimal coefficients for estimating B, there must be at least an error of ε_i to predict the error:

$$\left| B_i - \sum_{i=1}^{3} f_{ij}^* u_{fi} \right| \le \varepsilon_i \quad (36)$$

The parameter $\tilde{f}_{ij}$ is defined according to Eq. (37):

$$\tilde{f}_{ij} = f_{ij} - f_{ij}^* \quad (37)$$

From Equations (27, 37), we will have:

$$u_{ci} = \sum_{i=1}^{3} \tilde{f}_{ij} u_{fi} + \sum_{i=1}^{3} \tilde{f}_{ij}^* u_{fi} \quad i = 1.2.3 \quad (38)$$

The parameter σ_i^* is also selected so that Eq. (39) is established:

$$\varepsilon_i \le \sigma_i^* |s_i| \;\; i = 1.2.3 \quad (39)$$

Moreover, the parameter $\tilde{\sigma}_i$ is defined as Eq. (40):

$$\tilde{\sigma}_i = \sigma_i - \sigma_i^* \quad (40)$$

According to the calculations presented in Appendix A2, and by replacing the Equations (32) to (40) in the derivative of the Lyapunov function (31), the inequality of Eq. (41) was proved. Thus, according to the Lyapunov theorem, convergence, and stability of the proposed controller are proved for all of the three axes.

$$\dot{\boldsymbol{V}} \le -\sum_{i=1}^{3} a_i s_i^2 < 0 \;,\; a_i < 0 \quad i = 1.2.3 \quad (41)$$

3- 3- Design of the Fuzzy Controller of the torque control $\boldsymbol{u_f}$

A fuzzy control system is designed to create coupling torque between the axes. The equations proposed in this section are written for the yaw axis and the body. By converting the equations from ψ to ϕ and θ, they can be generalized to the pitch and roll axes. The s_ψ parameter in Eq. (21) represents the relative angle between the Yaw gimbal and the body. Inputs of the fuzzy system and the yaw motor torque (u_f) are considered as system outputs. Five membership functions are intended for fuzzy inputs. Fuzzy rules are written as follows:

Rule 1: If s is the NB value, then u_f is equal to the output NB.

Rule 2: If s is the NM value, then u_f is equal to the output NM.

Rule 3: If s is the ZO value, then u_f is equal to the output ZO.

Rule 4: If s is the PM value, then u_f is equal to the output PM.

Rule 5: If s is the PB value, then u_f is equal to the output PB.

The five membership functions of NB, NM, ZO, PM, and PB are considered for the input variable, as shown in Fig. 3. The membership functions are defined as linear and triangular functions. The fuzzy system is designed to meet the conditions of continuity, compatibility, and completeness. Continuity condition means that the output of the fuzzy system is not intermittent. Compatibility means that two or more fuzzy laws cannot have the same output. Completeness implies that at least one fuzzy rule should be activated for each value of input. Besides, the fuzzy groups of each fuzzy variable must cover the entire range, and for each value of the input variable, at least one fuzzy group must be activated.

The output of the fuzzy rule is determined using the weighted mean method according to Equation (43):

$$u_{fi} = \frac{\sum_{R=1}^{5} \phi_{iR}\mu_R(s_i)}{\sum_{R=1}^{5} \mu_R(s_i)} \quad i = 1.2.3 \quad (42)$$

The parameter R in this equation is the number of matching rules, $\mu_R(s_i)$ is the input of the membership function corresponding to the R matching rule. The $[f]_{adap}$ adaptive factor, which is obtained from adaptation law (30), compensates for dynamic coupling between ISP axes based on Equation (29). Thus, the fuzzy control torque section was defined according to Equation (43) for all three axes.

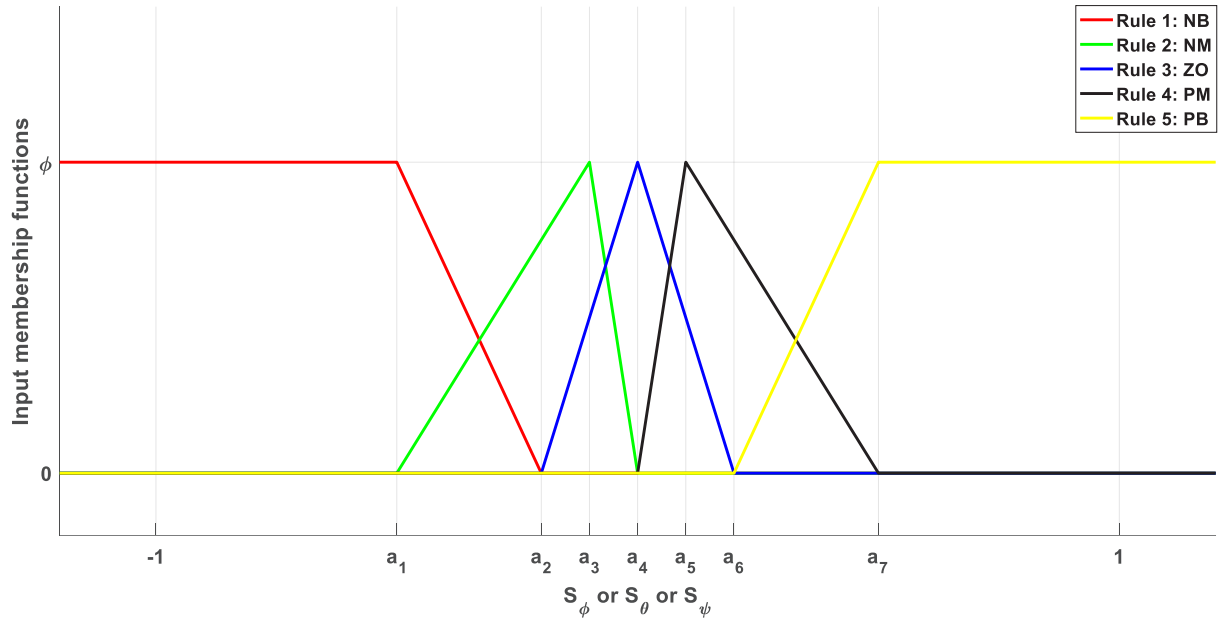

Fig. 3. Membership function of ϕ for rules one to five (NB, NM, ZO, PM, and PB).

4- Results and Discussions

To compare the applicability of the adaptive fuzzy controller with the PID method, the numerical simulation method has been used on the governing dynamic equations. The results of both controllers are presented in this section. System state variables refer to the relative angles of each gimbal, as defined in the schematics of Fig. 1b, as well as their rates $x = \begin{bmatrix} \dot{\phi} & \dot{\theta} & \dot{\psi} & \phi & \theta & \psi \end{bmatrix}$. Moreover, the torque calculated by the stabilized platform controller system $u = \begin{bmatrix} \tau_Y & \tau_P & \tau_R \end{bmatrix}$ is considered as the output of the dynamic system controller.

In the present simulation, the purpose of the designed controllers is to stabilize the system despite the movements of the stabilized platform's base and to bring the system state variables to the desired state x. In other words, the controller's main function is to maintain the line of sight (LOS) of the imaging sensor with respect to its inertial coordinates. In each simulation step, the desired angle is defined as an angle between the carrier of the ISP and the line of sight of the imaging sensor. Thus, the torques that are calculated by the controller and applied to the dynamic system have to minimize the platform stabilization error.

Dynamic system simulation starts with zero initial conditions (for all state variables). The parameters related to the gyroscopic stabilizer on which the simulation is performed are given in Table 2 and Table 3. Based on experimental tests of boat movements at sea, the ISP was simulated. These experimental data were used for ISP's base acceleration in each step of the simulation. For this purpose, the diagram of the movements of the platform's base in the three directions of roll, pitch, and yaw is shown in Fig. 4. Fig. 5. illustrates the tracking errors of the ISP relative angles when the proposed adaptive fuzzy controller is utilized. Fig. 6a shows the control actions required for roll, pitch, and yaw electric motors. Experimental tests were conducted by mounting ISP on a moving boat in the sea. Fig. 6b illustrates the errors of stabilization, which are defined as differences between the actual and desired relative angles of the frame.

Table 3 compares the results of using an adaptive fuzzy controller and the results of using a traditional PID controller. To evaluate the performance results of each controller, the Mean Absolute Error (MAE) was applied as a criterion according to Eq. (44):

$$MAE = \frac{\sum_{i=1}^{n} |e_i|}{n} \tag{43}$$

The results presented in the table below show that the use of the adaptive fuzzy controller has reduced the stabilization error of the roll, pitch, and yaw axes by 86%, 90%, and 94%, respectively in theory (simulation). Moreover, the stabilization errors of frames have been reduced by 66%, 85%, and 88%, respectively.

To compare the performance of the ISP controller with that of previous relevant literature, sinusoidal motion is applied to the carrier. A simulation method was used for comparison. According to the results, the proposed controller had the same control performance as the reference [19], which designed a controller for the roll axis in three perpendicular directions. The results indicate that designing controllers separately for three gimbals has no adverse effect on controller performance.

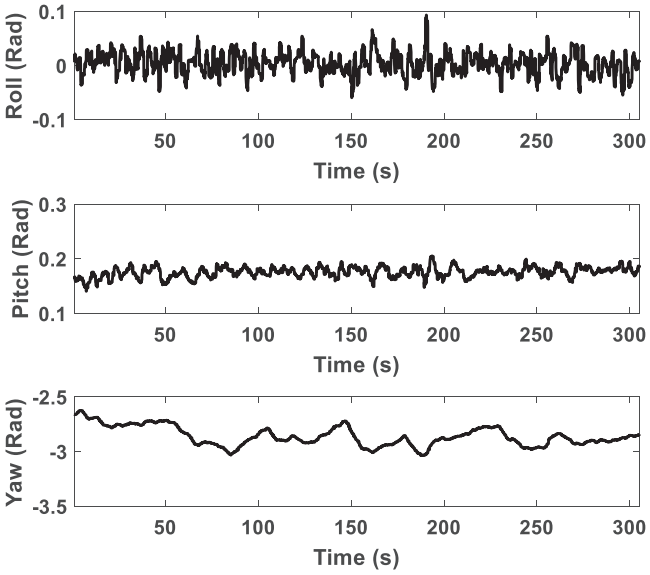

Fig. 4. Relative angle of the base's movement with respect to the axis of inertia coordinates in the direction of roll, pitch, and yaw.

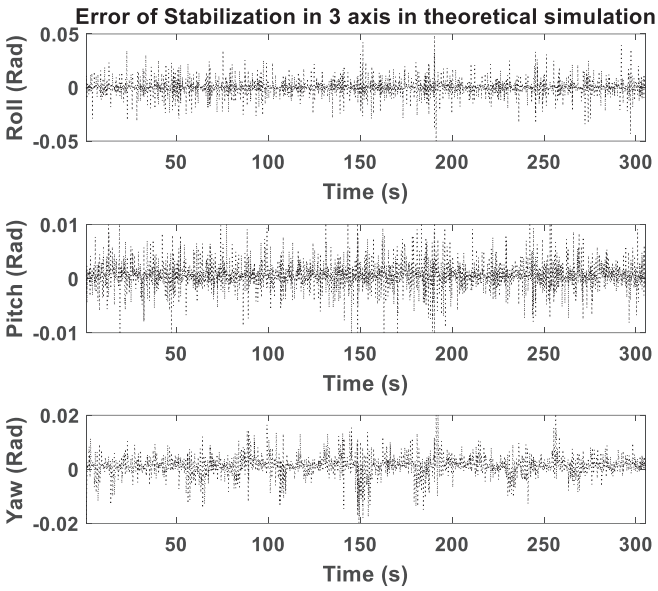

Fig. 5. The tracking error of the ISP angles in simulation. The difference between ISP angles and desired angles in numerical simulation.

Table 1. Comparison of the stabilization error of the adaptive fuzzy control algorithm with PID. A MAE criterion was employed.

Algorithm	Yaw (Rad)	Pitch (Rad)	Roll (Rad)
PID	4.8×10^{-2}	1.2×10^{-2}	2.2×10^{-2}
Feedforward compensation [23]	-	2×10^{-1}	1.5×10^{-1}
Dual closed-loop PID [3]	7.1×10^{-3}	7.8×10^{-3}	-
Internal model control [4]	1.1×10^{-2}	2×10^{-3}	-
Single axis model reference adaptive control [21]	1.7×10^{-2}	-	-
Single axis least mean square based ADRC [6]	4.7×10^{-4}	-	-
Combination of a backstepping with adaptive neural network [11] in case of carrier sinusoidal motion (single axis)	-	2.1×10^{-5}	-
Fuzzy-PID [24]	-	2.7×10^{-2}	2.4×10^{-2}
MIMO fuzzy controller [19]	6.1×10^{-4}	4.6×10^{-4}	3.3×10^{-4}
Fuzzy-adaptive (simulation)	2.7×10^{-3}	1.2×10^{-3}	3.1×10^{-3}
Fuzzy-adaptive (experiments)	5.8×10^{-3}	1.8×10^{-3}	7.5×10^{-3}
Fuzzy-adaptive (simulation) in case of carrier sinusoidal motion	5×10^{-4}	8×10^{-4}	2.3×10^{-4}

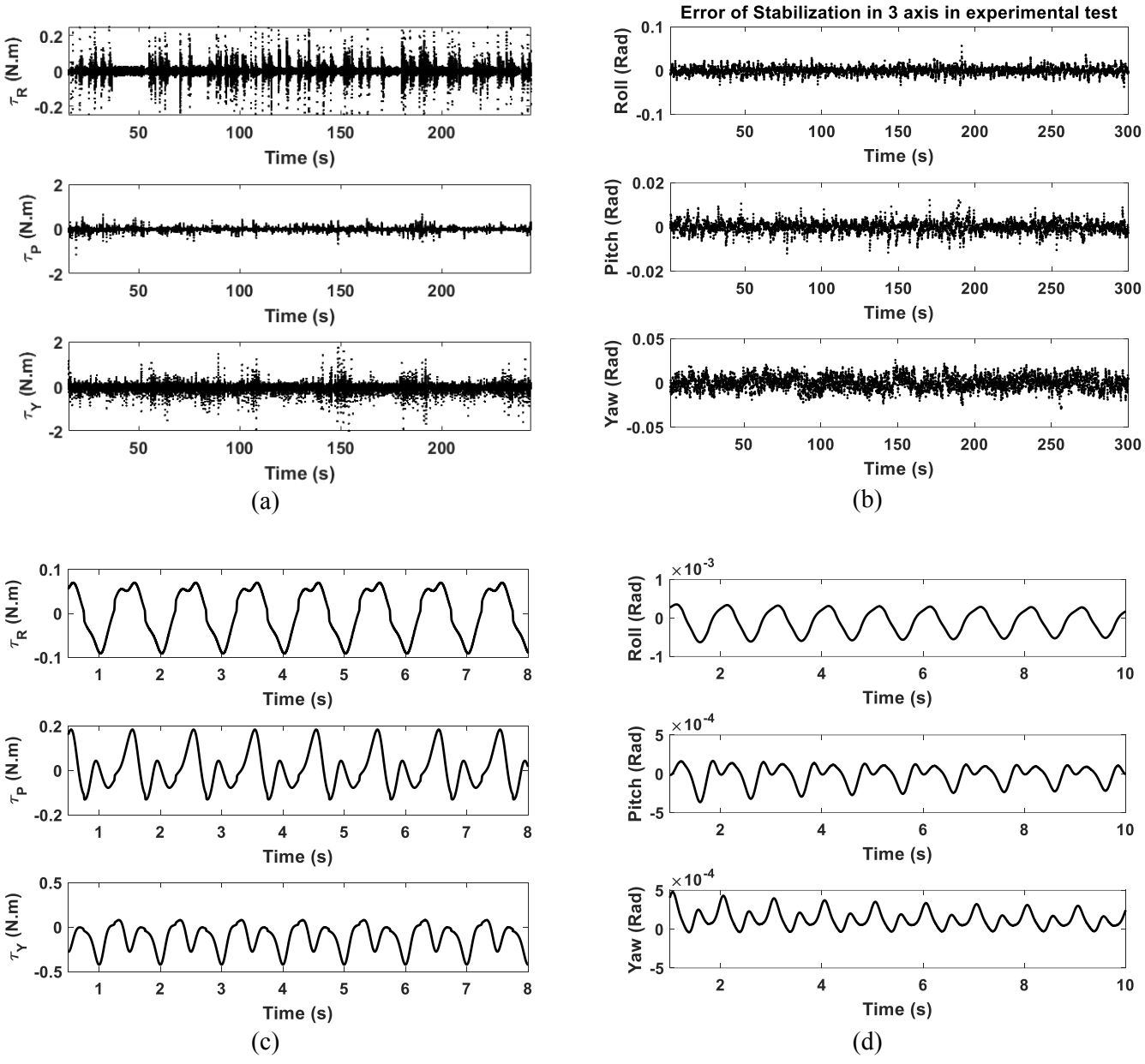

Fig. 6. (a) Control action needed to achieve desired performance using 3-DOF ISP. (b) Error of stabilization. The difference between ISP angles and desired angles in the experimental test. (c) Control action needed to achieve desired performance using 3-DOF ISP. (d) Error of stabilization. The difference between ISP angles and desired angles in the experimental test.

5- Conclusion

The present article investigated the dynamic modeling of a stable three-axis gyroscopic platform and developed an adaptive sliding mode fuzzy control system for it, considering the coupling between the axes. The fuzzy controller was designed based on a novel asymmetric membership function that enhances controller stabilization performance. To stabilize the platform, an adaptive fuzzy nonlinear controller and a PID linear controller were used separately. The process of designing and proving the stability of an adaptive fuzzy nonlinear controller is described. The performed simulation indicated that an adaptive sliding mode fuzzy controller had one order of magnitude better performance than the PID controller in the experimental test. The use of real movements for the base of the stabilized platform made the assessment of controller performance more realistic than previous researches. Hence, the results of simulations and experimental tests indicated that by using the proposed adaptive fuzzy controller, the stabilization error would be 90% less than using the PID controller.

Nomenclature

Table 2. Definition and naming the parameters used in dynamic equations (three-axis ISP)

Parameters	Value or definition
ω_B	the angular velocity of the body gimbal
M_{PRx}	Roll axis torque includes viscous friction, dry friction, and roll axis motor torque
M_{YPy}	Pitch axis torque includes viscous friction, dry friction, and pitch axis motor torque
M_{BYz}	Yaw axis torque includes viscous friction, dry friction, and yaw axis motor torque
MXR	Defined in the equation (53)
MYP	Defined in the equation (54)
MZY	Defined in the equation (55)
I_{ii}	The moment of inertia of the gimbals. The first term of their index identifies the name of the gimbal and the second term specifies the direction of the axis.
Moment of inertia of the roll axis gimbal in three directions	$I_{RX} = 4\times10^{-4}$,$I_{RY} = 2.53\times10^{-4}$, $I_{RZ} = 2.53\times10^{-4}$ kg.m^2
Moment of inertia of the pitch axis gimbal in three directions	$I_{PX} = 4.98\times10^{-3}$,$I_{PY} = 2.02\times10^{-3}$, $I_{PZ} = 3.46\times10^{-3}$ kg.m^2
Moment of inertia of the yaw axis gimbal in three directions	$I_{YX} = 6.55\times10^{-3}$,$I_{YY} = 1.46\times10^{-3}$, $I_{YZ} = 5.46\times10^{-3}$ kg.m^2
D_{PR}	Viscous friction between pitch and roll gimbals 0.01 N.m.s
$F_{PR}(sgn\dot{\phi})$	Coulomb friction and static friction representative function (related to tension in wiring) 0.01 N.m
τ_i	Motor torque of the roll (i = R), pitch (i = P), and yaw (i = Y) axes

Table 3. Values of the parameters of the proposed controller

Parameters	Value or definition
PID coefficient of roll gimbal	$K_D = 2, K_I = 20, K_P = 6$
PID coefficient of pitch gimbal	$K_D = 2, K_I = 6, K_P = 6$
PID coefficient of yaw gimbal	$K_D = 2, K_I = 20, K_P = 8$
Gamma matrix of the equation (28) γ	$\begin{bmatrix} 10 & 0 & 1 \\ 0 & 10 & 0 \\ 1 & 0 & 10 \end{bmatrix}$
Parameter η of the equation (29)	16
c matrix of the equation (18)	$\begin{bmatrix} 10 & 0 & 0 \\ 0 & 30 & 0 \\ 0 & 0 & 10 \end{bmatrix}$
"a" matrix of the equation (26)	$\begin{bmatrix} 1 & 0 & 0 \\ 0 & 3 & 0 \\ 0 & 0 & 1 \end{bmatrix}$
Fuzzy input range for the roll axis (S_ϕ) [a_1,a_2,a_3,a_4,a_5,a_6,a_7]	[-0.5 -0.2 -0.1 0 0.1 0.2 0.5]
Fuzzy input range for the pitch axis (S_θ) [a_1,a_2,a_3,a_4,a_5,a_6,a_7]	[-1 -0.6 -0.5 0 0.5 0.6 1]
Fuzzy input range for the yaw axis (S_ψ) [a_1,a_2,a_3,a_4,a_5,a_6,a_7]	[-7 -3 -1 0 1 3 7]
Φ value for the roll axis	$[-1 \quad -0.5 \quad 0 \quad 0.5 \quad 1]$
Φ value for the pitch axis	$[-3 \quad -1.5 \quad 0 \quad 1.5 \quad 3]$
Φ value for the yaw axis	$[-1 \quad -0.5 \quad 0 \quad 0.5 \quad 1]$

A. Appendix

A1- Extracting Dynamic Equations

This section includes Table 2 of the nomenclatures that are used in the dynamic equations. To obtain the dynamic equations of the three-axis ISP, we used the relations of reference [19]. It should be noted that friction on each axis is modeled as two components: viscous friction and Coulomb friction. The three equations of movement, namely Equations (44-46) can also be written as second-order differential equations in terms of system state variables as follows:

$$A_{R\phi}.\ddot{\phi} + A_{R\psi}.\ddot{\psi} = MXR \tag{1}$$

$$A_{P\theta}.\ddot{\theta} + A_{p\psi}.\ddot{\psi} = MYP \tag{2}$$

$$A_{Y\phi}.\ddot{\phi} + A_{Y\psi}.\ddot{\psi} + A_{Y\theta}.\ddot{\theta} = MZY \tag{3}$$

The other terms of the above equations are expressed as follows:

$$A_{R\phi} = I_{Rx} \tag{4}$$

$$A_{R\psi} = -s_\theta I_{Rx} \tag{5}$$

$$A_{P\theta} = I_{Py} + I_{Ry}c_\phi^2 + I_{Rz}s_\phi^2 \tag{6}$$

$$A_{p\psi} = c_\theta s_\phi c_\phi (I_{Ry} - I_{Rz}) \tag{7}$$

$$A_{Y\phi} = -I_{Rx}s_\theta \tag{8}$$

$$A_{Y\psi} = I_{Yz} - s_\theta^2(I_{px} - I_{Rx}) + c_\theta^2(I_{pz} + I_{Rz}c_\phi^2 + I_{Ry}s_\phi^2) \tag{9}$$

$$A_{Y\theta} = c_\theta s_\phi c_\phi (I_{Ry} - I_{Rz}) \tag{10}$$

$$\begin{aligned} MXR = M_{PRx} - I_{Rx}\{[(\dot{p} + q\dot{\psi})c_\psi + (\dot{q} - p\dot{\psi})s_\psi - (r + \dot{\psi})\dot{\theta}]c_\theta \\ + [-\dot{r} - (pc_\psi + qs_\psi)\dot{\theta}]s_\theta\} - (I_{Rz} - I_{Ry})\omega_{IRz}^R.\omega_{IRy}^R \end{aligned} \tag{11}$$

$$
\begin{aligned}
MYP = M_{YPy} - I_{Py}.\left[(\dot{q} - p\dot{\psi})c_{\psi} - (\dot{p} + q\dot{\psi})s_{\psi}\right] - (I_{Px} - I_{Pz})\omega_{IPx}^{P}.\omega_{IPz}^{P} \\
- c_{\phi}\Big(I_{Ry}\Big\{\{[\dot{r} + (pc_{\psi} + qs_{\psi})\dot{\theta}]c_{\theta} - (qc_{\psi} - ps_{\psi} + \dot{\theta})\dot{\phi} \\
+ [(\dot{q} - p\dot{\psi})s_{\psi} + (\dot{p} + q\dot{\psi})c_{\psi} - (r + \dot{\psi})\dot{\theta}]s_{\theta}\}s_{\phi} \\
+ \{(\dot{q} - p\dot{\psi})c_{\psi} - (\dot{p} + q\dot{\psi})s_{\psi} \\
+ [(r + \dot{\psi})c_{\theta} + (pc_{\psi} + qs_{\psi})s_{\theta}]\dot{\phi}\}c_{\phi}\Big\} + (I_{Rx} - I_{Rz})\omega_{IRx}^{R}.\omega_{IRz}^{R}\Big) \\
+ s_{\phi}\big(I_{Rz}(([\dot{r} + (pc_{\psi} + qs_{\psi})\dot{\theta}]c_{\theta} - (qc_{\psi} - ps_{\psi} + \dot{\theta})\dot{\phi} \\
+ [(\dot{q} - p\dot{\psi})s_{\psi} + (\dot{p} + q\dot{\psi})c_{\psi} - (r + \dot{\psi})\dot{\theta}]s_{\theta})c_{\phi} \\
- [(\dot{q} - p\dot{\psi})c_{\psi} - (\dot{p} + q\dot{\psi})s_{\psi} \\
+ [(r + \dot{\psi})c_{\theta} + (pc_{\psi} + qs_{\psi})s_{\theta}]\dot{\phi}]s_{\phi}) + (I_{Ry} - I_{Rx})\omega_{IRy}^{R}.\omega_{IRx}^{R}\big)
\end{aligned} \tag{12}
$$

$$
\begin{aligned}
ZY = M_{BYz} - I_{Yz}\dot{r} + (I_{Yy} - I_{Yx})\omega_{IYx}^{Y}.\omega_{IYy}^{Y} \\
+ s_{\theta}\big(I_{Px}.([(\dot{p} + q\dot{\psi})c_{\psi} + (\dot{q} - p\dot{\psi})s_{\psi} - (r + \dot{\psi})\dot{\theta}]c_{\theta} \\
+ [\dot{r} - (pc_{\psi} + qs_{\psi})\dot{\theta}]s_{\theta}) + (I_{Pz} - I_{Py})\omega_{IPz}^{P}.\omega_{IPy}^{P} \\
- I_{Rx}\{[(\dot{p} + q\dot{\psi})c_{\psi} + (\dot{q} - p\dot{\psi})s_{\psi} - (r + \dot{\psi})\dot{\theta}]c_{\theta} \\
+ [-\dot{r} - (pc_{\psi} + qs_{\psi})\dot{\theta}]s_{\theta}\} - (I_{Rz} - I_{Ry})\omega_{IRz}^{R}.\omega_{IRy}^{R}) \\
- c_{\theta}\Big(I_{Pz}.([(\dot{p} + q\dot{\psi})c_{\psi} + (\dot{q} - p\dot{\psi})s_{\psi} - (r + \dot{\psi})\dot{\theta}]s_{\theta} \\
+ [\dot{r} + (pc_{\psi} + qs_{\psi})\dot{\theta}]c_{\theta}) + (I_{Py} - I_{Px})\omega_{IPy}^{P}.\omega_{IPx}^{P} \\
+ s_{\phi}\Big(I_{Ry}\Big\{\{[\dot{r} + (pc_{\psi} + qs_{\psi})\dot{\theta}]c_{\theta} - (qc_{\psi} - ps_{\psi} + \dot{\theta})\dot{\phi} \\
+ [(\dot{q} - p\dot{\psi})s_{\psi} + (\dot{p} + q\dot{\psi})c_{\psi} - (r + \dot{\psi})\dot{\theta}]s_{\theta}\}s_{\phi} \\
+ \{(\dot{q} - p\dot{\psi})c_{\psi} - (\dot{p} + q\dot{\psi})s_{\psi} \\
+ [(r + \dot{\psi})c_{\theta} + (pc_{\psi} + qs_{\psi})s_{\theta}]\dot{\phi}\}c_{\phi}\Big\} + (I_{Rx} - I_{Rz})\omega_{IRx}^{R}.\omega_{IRz}^{R}\Big) \\
+ c_{\phi}\big(I_{Rz}(([\dot{r} + (pc_{\psi} + qs_{\psi})\dot{\theta}]c_{\theta} - (qc_{\psi} - ps_{\psi} + \dot{\theta})\dot{\phi} \\
+ [(\dot{q} - p\dot{\psi})s_{\psi} + (\dot{p} + q\dot{\psi})c_{\psi} - (r + \dot{\psi})\dot{\theta}]s_{\theta})c_{\phi} \\
- [(\dot{q} - p\dot{\psi})c_{\psi} - (\dot{p} + q\dot{\psi})s_{\psi} \\
+ [(r + \dot{\psi})c_{\theta} + (pc_{\psi} + qs_{\psi})s_{\theta}]\dot{\phi}]s_{\phi}) + (I_{Ry} - I_{Rx})\omega_{IRy}^{R}.\omega_{IRx}^{R}\big)\Big)
\end{aligned} \tag{13}
$$

$$M_{PRx} = -D_{PR}\dot{\phi} - F_{PR}(sgn\dot{\phi}) + \tau_{R} \tag{14}$$

$$M_{YPy} = -D_{YP}\dot{\theta} - F_{YP}(sgn\dot{\theta}) + \tau_{P} \tag{15}$$

$$M_{BYz} = -D_{BY}\dot{\psi} - F_{BY}(sgn\dot{\psi}) + \tau_{Y} \tag{16}$$

A2- Derivative Calculations of Lyapunov Function

By placing the equations, the Lyapunov function derivative will be obtained as Eq. (60):

$$\dot{V} = \sum_{i=1}^{3} s_i\left[B_i - a_i s_i - (\tilde{\sigma}_i + \sigma_i^*)s_i - \sum_{j=1}^{3} \tilde{f}_{ij} u_{fi} - \sum_{j=1}^{3} f_{ij}^* u_{fi}\right] + \sum_{i=1}^{3}\sum_{j=1}^{3}\left(\frac{1}{\gamma_{ij}}\tilde{f}_{ij}\dot{\tilde{f}}_{ij} - s_i\tilde{f}_{ij}u_{fi}\right) + \sum_{i=1}^{3}\left(\frac{1}{\eta_i}\tilde{\sigma}_i\dot{\tilde{\sigma}}_i - \tilde{\sigma}_i s_i^2\right) \tag{17}$$

By merging Equations (36) and (39), we will have:

$$s_i\left(B_i - \sum_{j=1}^{3} f_{ij}^* u_{fi}\right) \le |s_i|\left|B_i - \sum_{j=1}^{3} f_{ij}^* u_{fi}\right| \le |s_i| w_i \tag{18}$$

$$|s_i| w_i \le \sigma_i^* s_i^2 \tag{19}$$

Therefore, by placing the above equations in Eq. (60), we get:

$$\begin{aligned}\dot{\boldsymbol{V}} &\le -\sum_{i=1}^{3} a_i s_i^2 + \sum_{i=1}^{3}(|s_i|\varepsilon_i - s_i\sigma_i^* s_i) + \sum_{i=1}^{3}\sum_{j=1}^{3}\left(\frac{1}{\gamma_{ij}}\tilde{f}_{ij}\dot{\tilde{f}}_{ij} - s_i\tilde{f}_{ij}u_{fi}\right) + \sum_{i=1}^{3}\left(\frac{1}{\eta_i}\tilde{\sigma}_i\dot{\tilde{\sigma}}_i - \tilde{\sigma}_i s_i^2\right) \\ &\le -\sum_{i=1}^{3} a_i s_i^2 + \sum_{i=1}^{3}\sum_{j=1}^{3}\left(\frac{1}{\gamma_{ij}}\tilde{f}_{ij}\dot{\tilde{f}}_{ij} - s_i\tilde{f}_{ij}u_{fi}\right) + \sum_{i=1}^{3}\left(\frac{1}{\eta_i}\tilde{\sigma}_i\dot{\tilde{\sigma}}_i - \tilde{\sigma}_i s_i^2\right)\end{aligned} \tag{20}$$

The derivatives of equations (37, 40) are as follows:

$$\dot{\tilde{f}}_{ij} = \dot{f}_{ij} = \gamma_{ij} s_i u_{fi} \tag{21}$$

$$\dot{\tilde{\sigma}}_i = \dot{\sigma}_i = \eta_i s_i^2 \tag{22}$$

By placing the equation (64, 65) in the Lyapunov function, we will have:

$$\begin{aligned}\dot{\boldsymbol{V}} &\le -\sum_{i=1}^{3} a_i s_i^2 + \sum_{i=1}^{3}\sum_{j=1}^{3}\left(\frac{1}{\gamma_{ij}}\tilde{f}_{ij}\dot{\tilde{f}}_{ij} - s_i\tilde{f}_{ij}u_{fi}\right) + \sum_{i=1}^{3}\left(\frac{1}{\eta_i}\tilde{\sigma}_i\dot{\tilde{\sigma}}_i - \tilde{\sigma}_i s_i^2\right) \\ &= -\sum_{i=1}^{3} a_i s_i^2 + \sum_{i=1}^{3}\sum_{j=1}^{3}\left(\frac{1}{\gamma_{ij}}\tilde{f}_{ij}\gamma_{ij} s_i u_{fi} - s_i\tilde{f}_{ij}u_{fi}\right) \\ &\quad + \sum_{i=1}^{3}\left(\frac{1}{\eta_i}\tilde{\sigma}_i\eta_i s_i^2 - \tilde{\sigma}_i s_i^2\right) = -\sum_{i=1}^{3} a_i s_i^2\end{aligned} \tag{23}$$

References

[1] X. Lei, Y. Zou, F. Dong, A composite control method based on the adaptive RBFNN feedback control and the ESO for two-axis inertially stabilized platforms, ISA Trans., 59 (2015) 424-433.

[2] S. Leghmizi, L. Sheng, Kinematics modeling for satellite antenna dish stabilized platform, in: 2010 International Conference on Measuring Technology and Mechatronics Automation, IEEE, 2010, pp. 558-563.

[3] X. Zhou, Y. Jia, Q. Zhao, R. Yu, Experimental validation of a compound control scheme for a two-axis inertially stabilized platform with multi-sensors in an unmanned helicopter-based airborne power line inspection system, Sens., 16(3) (2016) 366.

[4] X. Zhou, H. Zhang, R. Yu, Decoupling control for two-axis inertially stabilized platform based on an inverse system and internal model control, Mechatronics, 24(8) (2014) 1203-1213.

[5] X.Liu, J.Mao, J.Yang, S.Li, K.Yang , Robust predictive visual servoing control for an inertially stabilized platform with uncertain kinematics. ISA transactions, 114 (2021) 347-358.

[6] C. Bai, Z. Zhang, A least mean square based active disturbance rejection control for an inertially stabilized platform, Optik, 174 (2018) 609-622.

[7] X. Zhou, Y. Jia, Q. Zhao, T. Cai, Dual-rate-loop control based on disturbance observer of angular acceleration for a three-axis aerial inertially stabilized platform, ISA Trans., 63 (2016) 288-298.

[8] O. Sushchenko, A. Tunik, Robust optimization of the inertially stabilized platforms, in: 2012 2nd International Conference" Methods and Systems of Navigation and Motion Control"(MSNMC), IEEE, 2012, pp. 101-105.

[9] J. Mao, J. Yang, X. Liu, S. Li, Q. Li, Modeling and robust continuous TSM control for an inertially stabilized platform with couplings, IEEE Transactions on Control Systems Technology, 28(6) (2019) 2548-2555.

[10] F. Wang, R. Wang, E. Liu, W. Zhang, Stabilization control mothed for two-axis inertially stabilized platform based on active disturbance rejection control with noise reduction disturbance observer, IEEE Access, 7 (2019) 99521-99529.

[11] Z. Ding, F. Zhao, Y. Lang, Z. Jiang, J. Zhu, Anti-disturbance neural-sliding mode control for inertially stabilized platform with actuator saturation, IEEE Access, 7 (2019) 92220-92231.

[12] J. Mao, S. Li, Q. Li, J. Yang, Design and implementation of continuous finite-time sliding mode control for 2-DOF inertially stabilized platform subject to multiple disturbances, ISA Trans., 84 (2019) 214-224.

[13] L.-D. Guo, Z.-F. Tan, Application of a sliding mode variable structure controller for stabilized platform of shipborne weapons, in: 2010 2nd IEEE International Conference on Information Management and Engineering, IEEE, 2010, pp. 65-68.

[14] F. Dong, X. Lei, W. Chou, A dynamic model and control method for a two-axis inertially stabilized platform, IEEE Transactions on Industrial Electronics, 64(1) (2016) 432-439.

[15] X. Zhou, B. Zhao, W. Liu, H. Yue, R. Yu, Y. Zhao, A compound scheme on parameters identification and adaptive compensation of nonlinear friction disturbance for the aerial inertially stabilized platform, ISA Trans., 67 (2017) 293-305.

[16] L.-X. Wang, A course in fuzzy systems and control, Prentice-Hall, Inc., 1996.

[17] L.-X. Wang, J.M. Mendel, Fuzzy basis functions, universal approximation, and orthogonal least-squares learning, IEEE Trans. Neural Networks, 3(5) (1992) 807-814.

[18] S. Leghmizi, S. Liu, A survey of fuzzy control for stabilized platforms, arXiv preprint arXiv:1109.0428, (2011)

[19] Z. Zhou, B. Zhang, D. Mao, MIMO fuzzy sliding mode control for three-axis inertially stabilized platform, Sens., 19(7) (2019) 1658.

[20] B.Xiang, and Q. Mu, Gimbal control of inertially stabilized platform for airborne remote sensing system based on adaptive RBFNN feedback model., IFAC Journal of Systems and Control, 16 (2021) 100148.

[21] X. Zhou, C. Yang, T. Cai, A model reference adaptive control/PID compound scheme on disturbance rejection for an aerial inertially stabilized platform, Journal of Sensors, 2016 (2016).

[22] Z. Hurák, M. Rezac, Image-based pointing and tracking for inertially stabilized airborne camera platform, IEEE Transactions on Control Systems Technology, 20(5) (2011) 1146-115923.

[23] X.Zhou, G.Gong and R.Yu, Decoupling control for a three-axis inertially stabilized platform used for aerial remote sensing. Transactions of the Institute of Measurement and Control, 37(9) (2015) 1135-1145.

[24] Y.Zhang, T.Yang, C.Li, S.Liu, C.Du, M.Li, Fuzzy-PID control for the position loop of aerial inertially stabilized platform. Aerospace Science and Technology, 36 (2014) 21-26.

HOW TO CITE THIS ARTICLE

M. Nikkhoo, H. Sayyaadi, M. S. Seif, Experimental Validation of Adaptive Sliding Mode Fuzzy Controller for an Inertially Stabilized Platform, AUT J. Elec. Eng., 55(3) (Special Issue) (2023) 333-350.

DOI: 10.22060/eej.2023.22068.5510